Structural instabilities of infinite-layer nickelates from first-principles simulations

Álvaro Adrián Carrasco Álvarez, Sébastien Petit, Lucia Iglesias, Manuel C Bibes, Julien Varignon, Wilfrid Prellier

Structural instabilities of infinite-layer nickelates from first-principles simulations

Álvaro Adrián Carrasco Álvarez,[1,2] Sébastien Petit,[1] Lucia Iglesias,[2] Wilfrid Prellier,[1] Manuel Bibes,[2] and Julien Varignon[1]

[1]*Laboratoire CRISMAT, Normandie Université, ENSICAEN, UNICAEN, Centre National de la Recherche Scientifique, 14000 Caen, France*
[2]*Unité Mixte de Physique, CNRS, Thales, Université Paris Saclay, 91767 Palaiseau, France*

(Received 9 December 2021; revised 4 February 2022; accepted 15 March 2022; published 22 April 2022)

Rare-earth nickelates RNiO$_2$ adopting an infinite-layer phase show superconductivity once La, Pr, or Nd is substituted by a divalent cation. Either in the pristine or doped form, these materials are reported to adopt a high-symmetry, perfectly symmetric, P_4/mmm tetragonal cell. Nevertheless, bulk compounds are scarce, hindering a full understanding of the role of chemical pressure or strain on lattice distortions that in turn could alter magnetic and electronic properties of the two-dimensional nickelates. Here, by performing a full analysis of the prototypical YNiO$_2$ compound with first-principles simulations, we identify that these materials are prone to exhibit O$_4$ group rotations whose type and amplitude are governed by the usual R-to-Ni cation size mismatch. We further show that these rotations can be easily tuned by external stimuli modifying lattice parameters such as pressure or strain. Finally, we reveal that H intercalation is favored for any infinite-layer nickelate member and pushes the propensity of the compounds to exhibit octahedra rotations.

DOI: 10.1103/PhysRevResearch.4.023064

I. INTRODUCTION

The nickelate oxides have long been proposed as potential candidates for high-temperature superconductivity [1,2]. However, superconductivity was only achieved recently after the RNiO$_3$ phase was doped with a divalent cation (Ca or Sr) and transformed into a RNiO$_2$ infinite-layer structure (R = La, Pr, or Nd) by reduction with CaH$_2$ [3–9]. Although the origin of superconductivity is yet to be clarified in these compounds, it was originally pointed out that $4f$ electrons in Nd$_{0.8}$Sr$_{0.2}$NiO$_2$ may play a key role [10]. This is, however, ruled out by the appearance of superconductivity in doped LaNiO$_2$ in which there are no $4f$ electrons. Thus, the occurrence of superconductivity in different infinite-layer nickelates suggests that this property may appear in any member of the family independently of the rare earth and of the presence of $4f$ electrons. So far, all observed superconducting nickelates (i.e., R = La, Pr, or Nd), exclusively obtained as thin films, are reported to crystallize within a highly symmetric, undistorted, P_4/mmm cell consisting of NiO$_2$ layers intercalated between rare-earth layers [11–14] [see Fig. 1(a)]. Nevertheless, experimental reports of infinite-layer nickelates with other R cations either in the bulk or thin film form are lacking. One may thus wonder whether the P_4/mmm structure is persistent across the whole family or if A-to-B cation size mismatch appearing in ABO$_3$ perovskites—quantified through the Goldschmidt tolerance factor [15] and yielding the usual octahedra rotations and potential gap opening in such compounds [16]—may appear in infinite-layer nickelates with small R cations.

Recent references have addressed this question from a theoretical point of view using the phonon dispersion curve of the infinite layer nickelates [17,18]. The authors identified the existence of a single O$_4$ group rotation yielding a $a^0a^0c^-$ rotation pattern [Ø mode in Fig. 1(c)] following Glazer's notation [19] in nickelate members with a small R cation such as YNiO$_2$. Furthermore, YNiO$_2$ was also proposed to disfavor H contamination that can potentially appear during the CaH$_2$ reduction process of the parent RNiO$_3$ phase [20,21]. Nevertheless, that study was guided by phonon calculations and neglects the potential lattice mode couplings that can help stabilizing different tilt patterns and/or antipolar motion of octahedra cations [16,22–24] such as those exhibited by the usual $Pbnm$ symmetry of ABO$_3$ perovskites ($Ø_z^+$, $Ø_{xy}^-$, and A_p modes displayed in Fig. 1).

We performed first-principles simulations using density functional theory (DFT) aiming at identifying the ground state structure of various nickelate members. We identify that compounds with small R cations such as YNiO$_2$ are prone to exhibit O$_4$ rotations yielding an orthorhombic $Pbnm$ symmetry of the form $a^-a^-c^+$. This behavior is reminiscent of the octahedra tilt pattern exhibited by most ABO$_3$ perovskite, including the parent RNiO$_3$ phase—except for LaNiO$_3$ [25]. In these members, a trilinear term between the $a^-a^-c^0$ ($Ø_{xy}^-$) and $a^0a^0c^+$ ($Ø_z^+$) rotations and an antipolar motion of R cations, allowed in the free energy expansion, lower the total energy and force their appearance in the ground state. Upon increasing the rare-earth radius such as in GdNiO$_2$, the O$_4$ groups tilt patterns change to $a^0a^0c^-$ within a I_4/mcm symmetry. This is induced by an unstable phonon mode overcoming the energy gain associated with the alternative tilt pattern yielding the $Pbnm$ symmetry. Structural distortions are absent for PrNiO$_2$ and LaNiO$_2$, and these adopt the high-symmetry,

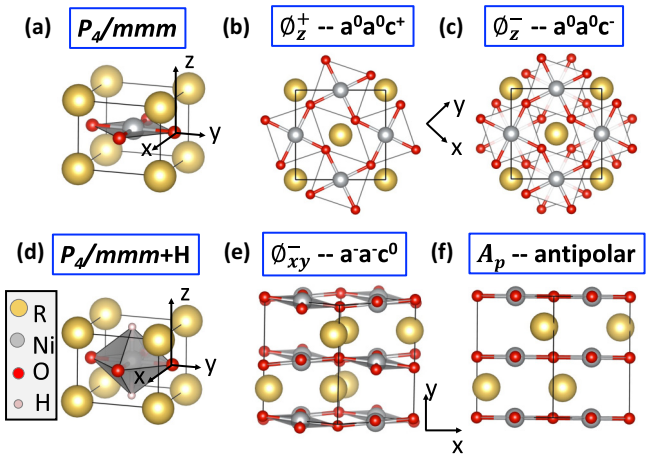

FIG. 1. Sketch of the different lattice distortions that can appear in the two-dimensional (2D) nickelates. (a) Highly symmetric undistorted P_4/mmm cell adopted by nickelates. (b) In-phase $a^0a^0c^+$ and (c) antiphase $a^0a^0c^-$ O_4 group rotations. (d) H intercalation at the apex of O_4 groups. (e) Antiphase $a^-a^-c^0$ rotation. (f) Antipolar motion A_p of R cations. We note that the antiphase rotation $a^-a^-c^0$ is also accompanied by an antipolar motion of A site cations.

totally undistorted, P_4/mmm cell. Finally, starting from the proper ground state structure, all materials prefer to stabilize hydrogen in the unit cell that in turn favor octahedra rotations and open a finite bandgap.

II. METHODS

First-principles DFT simulations are performed with the Vienna *Ab initio* Simulation Package (VASP) [26,27] using the recent Strongly Correlated and Appropriately Normalized (SCAN) functional [28] to better cancel self-interaction errors inherent to practiced DFT. It was previously shown to be well suited for ABO_3 compounds with a $3d$ element in bulk [29], including to treat doping effects in rare-earth nickelates [30] or in cuprates [31,32]. The explored structures are based on different tilt patterns of O_4 motifs that are defined using Glazer's notation [19]: it entails $a^0a^0c^+$ (P_4/mbm, $\emptyset_z^+$ mode), $a^-a^-c^0$ ($Imma$, $\emptyset_{xy}^-$ mode), $a^0a^0c^-$ (I_4/mcm, $\emptyset_z^-$ mode), $a^-a^-c^-$ (C_2/c, $\emptyset_z^- + \emptyset_{xy}^-$ modes), and $a^-a^-c^+$ ($Pbnm$, $\emptyset_z^+ + \emptyset_{xy}^-$ modes) tilt patterns. All calculations are performed using a $(\sqrt{2}, \sqrt{2}, 2)$ supercell (4 f.u.) with respect to the primitive, high-symmetry P_4/mmm cell. Here, $RNiO_2$ tested compounds cover R = Y, Gd, Pr, and La. Structural relaxation is performed until forces acting on each atom are <1 meV/Å. The energy cutoff is set to 650 eV, and the k-mesh is set to $8 \times 8 \times 6$ points for the 4 f.u. cell. Here, $4f$ electrons are treated in the simulations, and the magnetic order on both A and Ni cations is restricted to the AFM-C order previously identified with the SCAN functional [33].

III. RESULTS

A. Structural relaxation in $YNiO_2$

We first focus on $YNiO_2$ for which the parent perovskite phase $YNiO_3$ would show the largest A-to-B cation size mismatch among our considered compounds. Thus, one expects a larger propensity to exhibit O_4 group rotations. We summarize in Table I the total energy difference between all tested tilt patterns with respect to the undistorted high-symmetry P_4/mmm cell. The $Imma$ ($a^-a^-c^0$) and P_4/mbm ($a^0a^0c^+$) cells are found unstable and relax back to a P_4/mmm cell. It suggests that these tilt patterns alone are not stable in $YNiO_2$. For the other possibilities, we observe that $YNiO_2$ is nevertheless clearly prone to exhibit oxygen group rotations since the undistorted primitive P_4/mmm cell is less stable than all other tested cells. Among all tilt patterns, we identify the orthorhombic $Pbnm$ symmetry showing the usual $a^-a^-c^+$ O_4 group tilt patterns as the structural ground state. Our identification of an orthorhombic symmetry is in contrast with two recent DFT studies that found the I_4/mcm cell to be the structural ground state [17,18]. This discrepancy could be originated from a lower level of approximation of exchange-correlation (xc) phenomena through the used DFT xc functionals (i.e., PBEsol [34] or PBE [35] functionals). Nevertheless, we have tested the relative stability between $Pbnm$ and I_4/mcm symmetries with PBEsol and PBEsol + U ($U = 5$ eV on Ni $3d$ orbitals [36]) and still find that the $Pbnm$ cell is lower in energy than the I_4/mcm ($\Delta E = -27$ and -57 meV/f.u. for the energy difference, respectively).

TABLE I. Total energies differences (in meV/f.u.) with respect to the P_4/mmm cell for the different tilt patterns that could be stabilized in $YNiO_2$. Amplitudes of structural distortions (in Å/f.u.) of the different relaxed structure with respect to a high-symmetry P_4/mmm cell. Amplitudes are extracted from a symmetry mode analysis using AMPLIMODES software [37,38].

Symmetry	P_4/mmm	I_4/mcm	C_2/c	$Pbnm$
ΔE (meV/f.u.)	0	−175	−179	−212
$\emptyset_z^+$ ($a^0a^0c^+$, M_2^+)	–	–	–	0.593
$\emptyset_{xy}^-$ ($a^-a^-c^0$, A_5^-)	–	–	0.156	0.333
$\emptyset_z^-$ ($a^0a^0c^-$, A_4^-)	–	0.504	0.517	–
A_p (Z_5^-)	–	–	–	0.449

B. Avalanche effect produces the *Pbnm* cell in $YNiO_2$

Aiming at understanding the origin of the orthorhombic $Pbnm$ cell exhibited by $YNiO_2$, we first perform a symmetry mode analysis of our stabilized structures with respect to the high-symmetry P_4/mmm unit cell using the AMPLIMODE software [37,38] (see Table I). We see that the I_4/mcm and C_2/c cells only exhibit antiphase rotations, whereas the $Pbnm$ symmetry shows the $a^0a^0c^+$ ($\emptyset_z^+$) and $a^-a^-c^0$ ($\emptyset_{xy}^-$) plus the antipolar motion A_p of A site cations [Fig. 1(f)] identified in any $Pbnm$ cell of ABO_3 materials [16,23,24,39]. We then plot the potential energy surface associated with individual distortion modes, starting from the high-symmetry P_4/mmm cell with lattice parameters of the relaxed P_4/mmm cell [Fig. 2(a)]. As one can see, only the $a^0a^0c^-$ ($\emptyset_z^-$) mode presents a double well potential, while all other modes such as $a^-a^-c^0$ ($\emptyset_{xy}^-$) and $a^0a^0c^+$ ($\emptyset_z^+$) exhibit a single well potential. In other words, only the $\emptyset_z^-$ mode is unstable and is willing to appear spontaneously in the material. This result agrees with the results

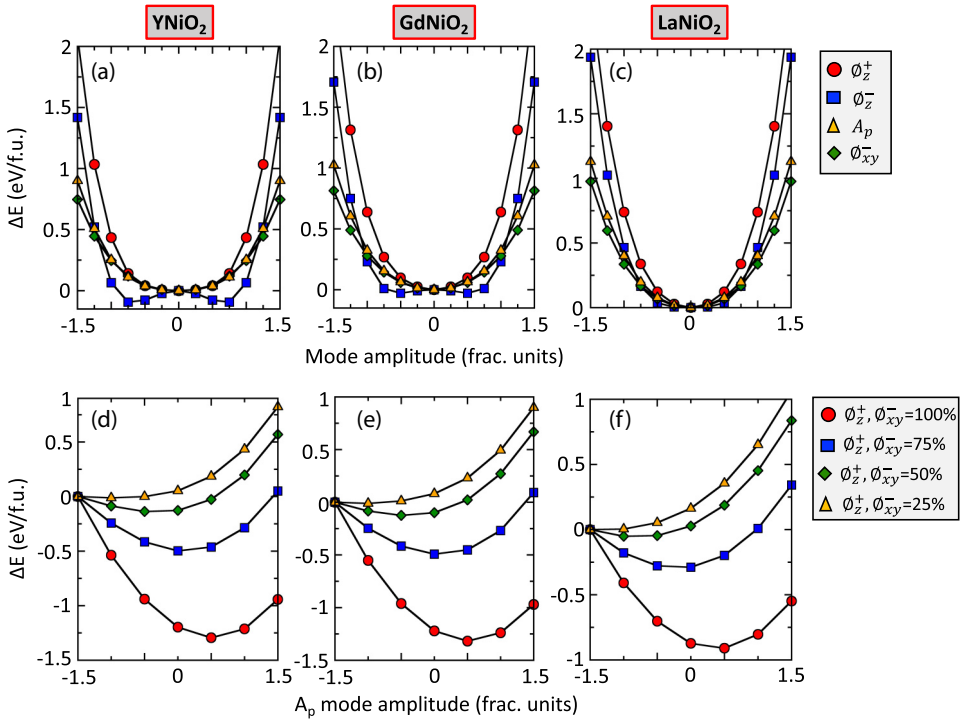

FIG. 2. Energy difference (in meV/f.u.) with respect to the P_4/mmm cell associated with the different lattice distortions that can appear in the two-dimensional (2D) nickelates tested in the simulations. (a)–(c) Potential energy surface associated for modes alone in $YNiO_2$, $GdNiO_2$, and $LaNiO_2$. (d)–(f) Potential energy surface associated with the antipolar mode A_p at fixed amplitude of the octahedra rotations.

of Bernardini *et al.* [17] as well as Xia *et al.* [18] that found a single instability associated with the $a^0a^0c^-$ rotation in the phonon dispersion curve of $YNiO_2$.

Thus, the next question is: How can the $a^0a^0c^+$ and $a^-a^-c^0$ tilt pattern be more stable than the $a^0a^0c^-$ tilt pattern in this compound if these two former modes are not unstable by themselves? To understand the stabilization of the *Pbnm* cell, we develop the free energy F associated with the distortions appearing in the ground state structure (i.e., $\emptyset_{xy}^-$, $\emptyset_z^+$, A_p) around the P_4/mmm cell:

$$F(Pbnm) \propto \alpha(\emptyset_z^+)^2 + \beta(\emptyset_z^+)^4 + \gamma(\emptyset_{xy}^-)^2 + \delta(\emptyset_{xy}^-)^4 + \lambda(A_p)^2 + \varsigma(A_p)^4 + \xi\emptyset_z^+\emptyset_{xy}^-A_p. \quad (1)$$

While even terms are expected in the free energy expansion of Eq. (1), we recover the trilinear term (i.e., an odd term) between $\emptyset_z^+$, $\emptyset_{xy}^-$, and A_p modes identified in ABO_3 perovskites adopting a *Pbnm* cell [16,22–24,40]. This term is only allowed within the *Pbnm* symmetry—or lower symmetries—and is absent in structures adopting $a^0a^0c^-$ or $a^-a^-c^-$ rotation patterns (i.e., I_4/mcm or C_2/c cells). The trilinear term has a surprising role in infinite-layer nickelates: by plotting the potential energy surface as a function of A_p but at fixed amplitudes of $\emptyset_z^+$ and $\emptyset_{xy}^-$ distortions, we see that, upon increasing amplitudes of $\emptyset_z^+$ and $\emptyset_{xy}^-$ distortions, the energy minimum is shifted to lower energies and finite amplitudes of the A_p mode [see Fig. 2(d)]. Although the $\emptyset_z^+$, $\emptyset_{xy}^-$, and A_p modes are all stable individually with respect to the P_4/mmm cell, the trilinear term possesses a strong and negative contribution to F in Eq. (1) that can produce the concomitant appearance of all three distortions despite these being not unstable by themselves. Thus, the *Pbnm* cell exhibited by $YNiO_2$ appears through an avalanche effect of *a priori* stable modes [41]. This lattice mode coupling then explains the discrepancy between our results and those of Refs. [17,18], in which lattice mode couplings were ignored.

C. Lattice relaxation effect on the stability of the *Pbnm* cell in $YNiO_2$

Although the identified trilinear term does explain the concomitant appearance of the $a^-a^-c^+$ O_4 group rotations by producing a large energy gain, it does not imply that it is the global minimum of the energy landscape as a function of the lattice distortion. Indeed, individual modes produce a large and positive contribution to the total energy that can counterbalance the negative contribution from the trilinear term of Eq. (1) as inferred by Fig. 2(a). Using the optimized P_4/mmm lattice parameter, we indeed observe that the *Pbnm* cell is not the ground state, this phase being higher in energy than the I_4/mcm cell by $\Delta E = +18.5$ meV/f.u. Allowing lattice parameters to relax in both symmetries, the cell can distort and adjust the rotation pattern. Consequently, a substantial energy gain is achieved by minimizing strain effects in the *Pbnm* symmetry, thereby allowing it to become 37 meV/f.u. lower than the I_4/mcm phase. One notices that, if we start from a P_4/mmm cell but at the *Pbnm* cell volume, the potential energy surface of the $\emptyset_z^+$ mode shows a double well potential, thereby further lowering the total energy of the compound.

D. Epitaxial strain effect in $YNiO_2$

Most of the infinite-layer nickelates realized so far are stabilized in thin film form. Having established that cell

distortions are a key parameter to reach the *Pbnm* cell in $YNiO_2$, one may thus wonder whether epitaxial strain effects may alter the stability of the *Pbnm* cell with respect to the I_4/mcm cell. Imposing the in-plane lattice constant of a relaxed cubic $SrTiO_3$ with the SCAN functional ($a_{STO} = 3.908$ Å), we find that the *Pbnm* cell remains the ground state, although its stability with respect to the I_4/mcm symmetry strongly diminishes ($\Delta E = -10$ meV/f.u.). We conclude here that strain is likely to disfavor the orthorhombic *Pbnm* cell.

E. Chemical pressure effect on the structural phase transition of other nickelate members

Since octahedra rotation amplitudes are governed by steric effects in ABO_3 perovskites, one may also wonder if these phenomena occur in the infinite-layer nickelates. We performed structural relaxation for a few other compounds such as $GdNiO_2$, $PrNiO_2$, and $LaNiO_2$, i.e., compounds with increasing A site cation radius. We identify that $GdNiO_2$ adopts a I_4/mcm ground state structure associated with only the $a^0a^0c^-$ O_4 group rotation ($\Delta E = -30$ meV/f.u. with respect to the *Pbnm* cell), while $PrNiO_2$ and $LaNiO_2$ exhibit a purely undistorted P_4/mmm cell as a ground state. In all these compounds, the trilinear term linking the in-phase $\emptyset_z^+$ and antiphase $\emptyset_{xy}^-$ rotation with an antipolar motion A_p remains effective, as shown in Fig. 2(e), and in fact, this trilinear term in Eq. (1) may always produce a negative contribution to the total energy, whatever the material. However, its energy gain cannot overcome the large positive contribution to the total energy of the individual $\emptyset_z^+$, $\emptyset_{xy}^-$, and A_p modes that still exhibit single wells [Figs. 2(b) and 2(c)]. As a result, $GdNiO_2$ only exhibits an antiphase octahedra rotation around the *c* axis ($a^0a^0c^-$) that arises from an unstable phonon in the P_4/mmm cell, as inferred from Fig. 2(b). In $LaNiO_2$, all distortion modes are found to be stable, including the antiphase $a^0a^0c^-$ rotation [Fig. 2(c)]. We conclude here that, akin to ABO_3 compounds, A-to-B cation size mismatch is still effective in reducing the crystal symmetry in the infinite-layer phase.

F. Hydrogen intercalation is found to be favored in all compounds

Since, experimentally, infinite-layer nickelates are obtained by a CaH_2 chemical reduction of the parent $RNiO_3$ perovskite phase, it is expected that some level of H intercalation may be present. Thus, we now examine the influence of this effect on phase stability. In $NdNiO_2$, it was proposed that the pristine phase is highly unstable, while its hydrogenation makes it more stable [21]. Recently, it was discussed that going to $YNiO_2$ [17] or decreasing the (*ab*)-plane P_4/mmm lattice parameter could disfavor H intercalation inside these nickelates [20]. These possibilities thereby offer a knob to get rid of H intercalation in the materials that ultimately can alter their properties. We have computed the binding energy for H intercalation at the apex of O_4 groups, which was found to be the preferred position in Refs. [17,21] [see Fig. 1(d)], considering the extreme limit of one H intercalated per primitive unit cell (i.e., $RNiO_2H$) using the following equation:

$$E_{\text{binding}} = E(R\text{NiO}_2\text{H}) - E(R\text{NiO}_2) - E(\text{H}). \qquad (2)$$

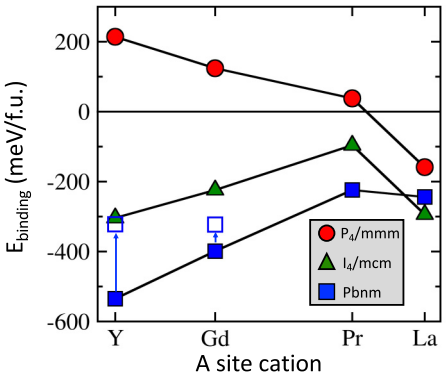

FIG. 3. Binding energy (in meV/f.u.) for hydrogen intercalation in the different two-dimensional (2D) nickelates. The reference energy is set to pristine material with the P_4/mmm space group. Arrows correspond to the binding energy for the hydrogenated *Pbnm* cell computed with respect to the ground state structure of the pristine phase for $YNiO_2$ and $GdNiO_2$ (blue open squares).

In Eq. (2), we consider total energies obtained after structural relaxation for $RNiO_2H$ and $RNiO_2$. The reference for the total energy of hydrogen is set to half the total energy of relaxed H_2 with the SCAN functional. From Eq. (2), it follows that a negative (positive) value for E_{binding} indicates a favorable (unfavorable) hydrogen intercalation in the material.

Trends for E_{binding} as a function of the rare-earth are reported in Fig. 3. Using the pristine P_4/mmm structure as a reference energy for all nickelate members, the binding energy for intercalating hydrogen is positive for $YNiO_2$ and then decreases upon increasing the radius of the A site cation, until it becomes negative only for $LaNiO_2$. This is compatible with the result of Ref. [20] that found H intercalation to be favorable in $LaNiO_2$. Thus, from the strict point of view of the high-symmetry, undistorted P_4/mmm cell, $LaNiO_2$ would be the only member to favor stabilization of H inside the cell during the CaH_2 chemical reduction process. Nevertheless, we have tested the I_4/mcm and *Pbnm* symmetries with H intercalated and identified that both distorted cells produce large energy gains with respect to the P_4/mmm cell that in turn strongly favors H intercalation. The result remains valid even if one considers the pristine *Pbnm* or I_4/mcm ground state as a reference energy for $YNiO_2$ and $GdNiO_2$, respectively (see rescaled values indicated by arrows in Fig. 3). Consequently, unlike results from Ref. [17] where H inclusion is proposed to be ruled out in $YNiO_2$—shall it adopt the P_4/mmm symmetry—we clearly identify that, once using the proper distorted cell for each nickelate member, all nickelates have negative binding energies toward the insertion of H, with a mean value of -290 meV/f.u. across the series. Although our simulations are restricted to the extreme limit of 1 H inserted per primitive cell, it is therefore very likely that fractions of H tend to be trapped inside the infinite layer nickelate, whatever the A site cation. Investigation of intermediate H doping contents that may appear experimentally require larger supercell and is left for future studies.

Several side effects of the inclusion of hydrogen in the material have to be pointed out: (i) intercalating H in all nickelate members favors the appearance of octahedra rotation with

notably a tilt pattern around the c axis that is reminiscent of the parent $RNiO_3$ phase with $a^0a^0c^+$ rotations for all members except for R = La in which the $a^0a^0c^-$ rotation is found more stable, and (ii) H acts as an acceptor [21] and (iii) favors the appearance of a high-spin Ni^{2+} state with a magnetic moment of 1.5 μ_B—it is lower than the expected value of 2 μ_B due to spillage on surrounding O and H atoms. All these effects have the tendency to open a small but finite bandgap in all nickelates that are otherwise found metallic in the undoped phase [21].

IV. CONCLUSIONS

We have identified that steric effects play an important role in the structure of infinite-layer nickelates and that most members will show O_4 groups rotation producing either the usual orthorhombic $Pbnm$ symmetry for A site cations with small radius or an I_4/mcm symmetry for A site cations with moderate radius. Only members with the largest rare earth (R = La, Pr, or Nd), for which superconductivity is reported so far, adopt a perfectly undistorted cell in the pristine phase. Finally, we have clarified that these rotations favor H intercalation in the material that in turn increases rotation amplitude, ultimately resulting in an insulating phase with only Ni^{2+} cations in a high-spin state. This hints at the fact that a fraction of H may be intercalated and that doping with a divalent cation may be required to annihilate the incipient insulating behavior, as observed in the resistivity curve of undoped $NdNiO_2$ compound [3].

ACKNOWLEDGMENTS

This paper has received financial support from the CNRS through the Mission for Transversal and Interdisciplinary Initiatives interdisciplinary programs under the Project SuNi and through the ANR SUPERNICKEL. Authors acknowledge access granted to high-performance computing resources of Criann through the Projects No. 2020005 and No. 2007013 and of Cines through the DARI Project No. A0080911453. L.I. acknowledges funding from the Ile de France region and the European Union's Horizon 2020 research and innovation programme under the Marie Sklodowska-Curie Grant Agreement No. 21004513 (DOPNICKS Project).

[1] V. I. Anisimov, D. Bukhvalov, and T. M. Rice, Electronic structure of possible nickelate analogs to the cuprates, Phys. Rev. B **59**, 7901 (1999).

[2] P. Hansmann, X. Yang, A. Toschi, G. Khaliullin, O. K. Andersen, and K. Held, Turning a Nickelate Fermi Surface into a Cupratelike One through Heterostructuring, Phys. Rev. Lett. **103**, 016401 (2009).

[3] D. Li, K. Lee, B. Y. Wang, M. Osada, S. Crossley, H. R. Lee, Y. Cui, Y. Hikita, and H. Y. Hwang, Superconductivity in an infinite-layer nickelate, Nature (London) **572**, 624 (2019).

[4] X. Ren, Q. Gao, Y. Zhao, H. Luo, X. Zhou, and Z. Zhu, Strain-induced enhancement of Tc in infinite-layer $Pr_{0.8}Sr_{0.2}NiO_2$ films, arXiv:2109.057601 (2021).

[5] S. Zeng, C. Li, L. E. Chow, Y. Cao, Z. Zhang, C. S. Tang, X. Yin, Z. S. Lim, J. Hu, P. Yang *et al.*, Superconductivity in infinite-layer nickelate $La_{1-x}Ca_xNiO_2$ thin films, Sci. Adv. **8**, eabl9927 (2022).

[6] M. Osada, B. Y. Wang, B. H. Goodge, K. Lee, H. Yoon, K. Sakuma, D. Li, M. Miura, L. F. Kourkoutis, H. Y. Hwang, M. Osada, and H. Y. Hwang, A superconducting praseodymium nickelate with infinite layer structure, Nano Lett. **20**, 5735 (2020).

[7] P. Puphal, Y.-M. Wu, K. Fürsich, H. Lee, M. Pakdaman, J. A. N. Bruin, J. Nuss, Y. E. Suyolcu, P. A. van Aken, B. Keimer, M. Isobe, and M. Hepting, Topotactic transformation of single crystals: From perovskite to infinite-layer nickelates, Sci. Adv. **7**, eabl8091 (2021).

[8] M. Osada, B. Y. Wang, K. Lee, D. Li, and H. Y. Hwang, Phase diagram of infinite layer praseodymium nickelate $Pr_{1-x}Sr_xNiO_2$ thin films, Phys. Rev. Materials **4**, 121801(R) (2020).

[9] M. Osada, B. Y. Wang, B. H. Goodge, S. P. Harvey, K. Lee, D. Li, L. F. Kourkoutis, and H. Y. Hwang, Nickelate superconductivity without rare-earth magnetism: $(La, Sr)NiO_2$, Adv. Mater. **33**, 2104083 (2021).

[10] M. Y. Choi, K. W. Lee, and W. E. Pickett, Role of 4f states in infinite-layer $NdNiO_2$, Phys. Rev. B **101**, 020503(R) (2020).

[11] M. A. Hayward, M. A. Green, M. J. Rosseinsky, and J. Sloan, Sodium hydride as a powerful reducing agent for topotactic oxide deintercalation: Synthesis and characterization of the nickel (i) oxide $LaNiO_2$, J. Am. Chem. Soc. **121**, 8843 (1999).

[12] A. Ikeda, Y. Krockenberger, H. Irie, M. Naito, and H. Yamamoto, Direct observation of infinite NiO_2 planes in $LaNiO_2$ films, Appl. Phys. Express **9**, 061101 (2016).

[13] T. Takamatsu, M. Kato, T. Noji, and Y. Koike, Low temperature synthesis of the infinite-layer compound $LaNiO_2$ by soft-chemical techniques, Jpn. J. Appl. Phys. **49**, 093101 (2010).

[14] H. Lin, D. J. Gawryluk, Y. M. Klein, S. Huangfu, E. Pomjakushina, F. von Rohr, and A. Schilling, Universal spin-glass behaviour in bulk $LaNiO_2$, $PrNiO_2$ and $NdNiO_2$, New J. Phys. **24**, 013022 (2022).

[15] V. M. Goldschmidt, Die gesetze der krystallochemie, Naturwissenschaften, Naturwissenschaften **14**, 477 (1926).

[16] J. Varignon, M. Bibes, and A. Zunger, Origin of band gaps in 3 d perovskite oxides, Nat. Commun. **10**, 1658 (2019).

[17] F. Bernardini, A. Bosin, and A. Cano, Geometric effects in the infinite-layer nickelates, arXiv:2110.13580 (2021).

[18] C. Xia, J. Wu, Y. Chen, and H. Chen, Dynamical structural instability and its implications for the physical properties of infinite-layer nickelates, Phys. Rev. B **105**, 115134 (2022).

[19] A. M. Glazer, The classification of tilted octahedra in perovskite, Acta Crystallogr. B **28**, 3384 (1972).

[20] L. Si, W. Xiao, J. Kaufmann, J. M. Tomczak, Y. Lu, Z. Zhong, and K. Held, Topotactic Hydrogen in Nickelate Superconductors and Akin Infinite-Layer Oxides ABO_2, Phys. Rev. Lett. **124**, 166402 (2020).

[21] O. I. Malyi, J. Varignon, and A. Zunger, Bulk $NdNiO_2$ is thermodynamically unstable with respect to decomposition while hydrogenation reduces the instability and transforms it from metal to insulator, Phys. Rev. B **105**, 014106 (2022).

[22] J. Varignon, M. Bibes, and A. Zunger, Origins versus fingerprints of the Jahn-Teller effect in d-electron AbX_3 perovskites, Phys. Rev. Research **1**, 033131 (2019).

[23] J. Varignon, M. N. Grisolia, D. Preziosi, P. Ghosez, and M. Bibes, Origin of the orbital and spin ordering in rare earth titanates, Phys. Rev. B **96**, 235106 (2017).

[24] J. Varignon, N. C. Bristowe, E. Bousquet, and P. Ghosez, Coupling and electrical control of structural, orbital and magnetic orders in perovskites, Sci. Rep. **5**, 15364 (2015).

[25] S. Catalano, M. Gibert, J. Fowlie, J. Iñiguez, J. M. Triscone, and J. Kreisel, Rare-earth nickelates $RNiO_3$: thin films and heterostructures, Rep. Prog. Phys. **81**, 46501 (2018).

[26] G. Kresse and J. Hafner, *Ab initio* molecular dynamics for liquid metals, Phys. Rev. B **47**, 558 (1993).

[27] G. Kresse and J. Furthmüller, Efficiency of ab-initio total energy calculations for metals and semiconductors using a plane-wave basis set, Comput. Mater. Sci. **6**, 15 (1996).

[28] J. Sun, A. Ruzsinszky, and J. P. Perdew, Strongly Constrained and Appropriately Normed Semilocal Density Functional, Phys. Rev. Lett. **115**, 036402 (2015).

[29] J. Varignon, M. Bibes, and A. Zunger, Mott gapping in 3d ABO_3 perovskites without Mott-Hubbard interelectronic repulsion energy U, Phys. Rev. B **100**, 035119 (2019).

[30] L. Iglesias, M. Bibes, and J. Varignon, First-principles study of electron and hole doping effects in perovskite nickelates, Phys. Rev. B **104**, 035123 (2021).

[31] J. W. Furness, Y. Zhang, C. Lane, I. G. Buda, B. Barbiellini, R. S. Markiewicz, A. Bansil, and J. Sun, An accurate first-principles treatment of doping-dependent electronic structure of high-temperature cuprate superconductors, Commun. Phys. **1**, 11 (2018).

[32] C. Lane, J. W. Furness, I. G. Buda, Y. Zhang, R. S. Markiewicz, B. Barbiellini, J. Sun, and A. Bansil, Antiferromagnetic ground state of La_2CuO_4: A parameter-free *ab initio* description, Phys. Rev. B **98**, 125140 (2018).

[33] R. Zhang, C. Lane, B. Singh, J. Nokelainen, B. Barbiellini, R. S. Markiewicz, A. Bansil, and J. Sun, Magnetic and f-electron effects in $LaNiO_2$ and $NdNiO_2$ nickelates with cuprate-like $3d_{x^2-y^2}$ band, Commun. Phys. **4**, 118 (2021).

[34] J. P. Perdew, A. Ruzsinszky, G. I. Csonka, O. A. Vydrov, G. E. Scuseria, L. A. Constantin, X. Zhou, and K. Burke, Restoring the Density-Gradient Expansion for Exchange in Solids and Surfaces, Phys. Rev. Lett. **100**, 136406 (2008).

[35] J. P. Perdew, K. Burke, and M. Ernzerhof, Generalized Gradient Approximation Made Simple, Phys. Rev. Lett. **77**, 3865 (1996).

[36] S. L. Dudarev, G. A. Botton, S. Y. Savrasov, C. J. Humphreys, and A. P. Sutton, Electron-energy-loss spectra and the structural stability of nickel oxide: An LSDA+U study, Phys. Rev. B **57**, 1505 (1998).

[37] D. Orobengoa, C. Capillas, I. Aroyo, and J. M. Perez, Amplimodes: Symmetry-mode analysis on the bilbao crystallographic server, J. Appl. Crystallogr. **42**, 820 (2009).

[38] J. M. Perez-Mato, D. Orobengoa, and M. I. Aroyo, Mode crystallography of distorted structures, Acta Crystallogr. A **66**, 558 (2010).

[39] J. Varignon, N. C. Bristowe, and P. Ghosez, Electric Field Control of Jahn-Teller Distortions in Bulk Perovskites, Phys. Rev. Lett. **116**, 057602 (2016).

[40] J. M. Rondinelli and C. J. Fennie, Octahedral rotation-induced ferroelectricity in cation ordered perovskites, Adv. Mater. **24**, 1961 (2012).

[41] I. Etxebarria, J. M. Perez-Mato, and P. Boullay, The role of trilinear couplings in the phase transitions of aurivillius compounds, Ferroelectrics **401**, 17 (2010).